SANDIA REPORT
SAND2010-1147
Unlimited Release
Printed March 2010

Preliminary Performance Assessment of Biotoxin Detection for UWS Applications using a μChemLab Device

Isaac R. Shokair, Victoria A. VanderNoot, Ronald F. Renzi and Brent L. Haroldsen

Prepared by
Sandia National Laboratories
Albuquerque, New Mexico 87185 and Livermore, California 94550

Sandia is a multiprogram laboratory operated by Sandia Corporation,
a Lockheed Martin Company, for the United States Department of Energy's
National Nuclear Security Administration under Contract DE-AC04-94AL85000.

Approved for public release; further dissemination unlimited.

Issued by Sandia National Laboratories, operated for the United States Department of Energy by Sandia Corporation.

NOTICE: This report was prepared as an account of work sponsored by an agency of the United States Government. Neither the United States Government, nor any agency thereof, nor any of their employees, nor any of their contractors, subcontractors, or their employees, make any warranty, express or implied, or assume any legal liability or responsibility for the accuracy, completeness, or usefulness of any information, apparatus, product, or process disclosed, or represent that its use would not infringe privately owned rights. Reference herein to any specific commercial product, process, or service by trade name, trademark, manufacturer, or otherwise, does not necessarily constitute or imply its endorsement, recommendation, or favoring by the United States Government, any agency thereof, or any of their contractors or subcontractors. The views and opinions expressed herein do not necessarily state or reflect those of the United States Government, any agency thereof, or any of their contractors.

Printed in the United States of America. This report has been reproduced directly from the best available copy.

Available to DOE and DOE contractors from
U.S. Department of Energy
Office of Scientific and Technical Information
P.O. Box 62
Oak Ridge, TN 37831

Telephone: (865) 576-8401
Facsimile: (865) 576-5728
E-Mail: reports@adonis.osti.gov
Online ordering: http://www.osti.gov/bridge

Available to the public from
U.S. Department of Commerce
National Technical Information Service
5285 Port Royal Rd.
Springfield, VA 22161

Telephone: (800) 553-6847
Facsimile: (703) 605-6900
E-Mail: orders@ntis.fedworld.gov
Online order: http://www.ntis.gov/help/ordermethods.asp?loc=7-4-0#online

SAND2010-1147
Unlimited Release
Printed March 2010

Preliminary Performance Assessment of Biotoxin Detection for UWS Applications using a μChemLab Device

Isaac R. Shokair and Brent L. Haroldsen
Exploratory Systems Technologies

Victoria A. VanderNoot
Biosystems Research and Development

Ronald F. Renzi
Advanced Systems Engineering and Deployment

Sandia National Laboratories
Mail Stop 9104
P. O. Box 0969
Livermore, CA 94551-0969

Abstract

In a multiyear research agreement with Tenix Investments Pty. Ltd., Sandia has been developing field deployable technologies for detection of biotoxins in water supply systems. The unattended water sensor or UWS employs microfluidic chip based gel electrophoresis for monitoring biological analytes in a small integrated sensor platform. This instrument collects, prepares, and analyzes water samples in an automated manner. Sample analysis is done using the μChemLab™ analysis module. This report uses analysis results of two datasets collected using the UWS to estimate performance of the device. The first dataset is made up of samples containing ricin at varying concentrations and is used for assessing instrument response and detection probability. The second dataset is comprised of analyses of water samples collected at a water utility which are used to assess the false positive probability. The analyses of the two sets are used to estimate the Receiver Operating Characteristic or ROC curves for the device at one set of operational and detection algorithm parameters. For these parameters and based on a statistical estimate, the ricin probability of detection is about 0.9 at a concentration of 5 nM for a false positive probability of $1x10^{-6}$.

Acknowledgements

This work was funded through a Cooperative Research and Development Agreement (CRADA) with Tenix and CH2M Hill. The authors gratefully acknowledge the cooperation of the Contra Costa Water district (Alameda County, CA) and the City of Glendale Water Utility (Glendale, AZ) for allowing temporary installation of UWS prototypes in their respective water pumping stations. The authors also acknowledge the team of researchers and engineers at Sandia who have contributed to the instrument development and data collection. We also would like to thank Larry Thorne for his careful review of this report and for the useful feedback he provided.

Contents

I. Introduction

Sandia Laboratories has been involved in a multiyear research agreement with Tenix Investments Pty. Ltd. for the development of field deployable technologies for detection of biological contaminants in water supply systems.

The unattended water sensor or UWS was developed under this agreement. This device is based on the liquid-phase µ ChemLab™ technology[1-3] and employs microfluidic chip-based gel electrophoresis (CGE) for monitoring biological analytes in a small integrated sensor platform. The instrument is comprised of a sample probe for collecting a sample from the main water flow; a microfluidic sample preparation module employing Sandia designed fittings, microfluidic pumps and electrically actuated valves; and the µ ChemLab™ sample analysis module, which couples capillary electrophoresis separations with sensitive laser induced fluorescence detection. The system design uses a flexible architecture that can be adapted to a variety of applications through combination of microfluidic chip detection and a suite of microfluidic components.

The UWS system is controlled from a laptop or tablet computer using LabVIEW software, to analyze water samples about every 12 minutes. Key UWS design features provide for reliable long-term operation and ease of use. They include automation of the sample preparation steps such as mixing with detergent and rapid fluorescent labeling of the proteins, and automation of the detection and data analysis. Alarms and results of the analyses are sent to users via wireless communication, although the system could also be connected to a utility's monitoring system. Pressure transducers and a positive control verify correct functioning of the system. A 2-color laser induced fluorescence (LIF) module with internal standards allows corrections to migration time. This was found to be especially important for field operations where the ambient temperature changed. The standards used are ovalbumin (OVA), bovine serum albumin (BSA) and cholecystokinin peptide (CCK) and were prelabeled with Alexa Fluor 647. A 7-mW, 635-nm laser (Sanyo, Japan) was used for excitation of fluorescence near 650 nm. The channel for standards is referred to as the "red" channel.

The initial UWS prototype is configured to detect protein biotoxins such as ricin and staphylococcal enterotoxin B as a first step toward a total bioanalysis capability based on protein detection and protein profiling. The analyte sample is interrogated using a 5-mW, 405-nm laser (Sanyo, Japan) to detect fluorescamine-labeled sample proteins. The fluorescence is detected near 470 nm and thus the analyte channel is referred to as the "blue" channel.

This report considers analysis of the collected data and uses the analysis results to estimate detection probabilities for a given set of detection algorithm parameters and the instrument response for measurements containing ricin at several concentrations. The same detection parameters are also used to statistically estimate the probability of false detections. For all analysis the Adaptive Background Suppression-Peak Detection algorithm[4] is used to fit the signal backgrounds and detect and estimate peak parameters.

For estimation of false detection probabilities, measurements of collected water samples at the utilities were used. These samples were filtered to remove particulate matter larger than about 0.2 µm and therefore bacteria and viruses are removed and only individual soluble proteins are

allowed to pass through. In these measurements there were no observable interferent proteins present and thus no information is available on the probability of possible interferents in the ricin time region. Thus for the present analysis the probability of false positives due to interferents will not be considered and only false positives due to measurement noise and artifacts, or background suppression errors are considered.

II. Detection Analysis

The data analyzed in this report was collected on 2-color CGE μChemLab devices. The first channel ("red") is dedicated to separation of three calibration standards (CCK, OVA, and BSA). The "blue" channel is dedicated to analyte detection. The first set of measurements used in this report was collected with ricin present at varying concentrations. A total of 29 measurements at six different concentrations were collected. This data will be used for assessing the detection probability. The second set of data is a collection of measurements of water samples at CCWD and will be used for assessing the probability of false detections.

Analyte detection is based on a two step process. The first step uses the Adaptive Background Suppression-Peak Detection (ABS-PD) algorithm to iteratively fit the background and detect peaks. The second step applies linear chemometric analysis using classical least squares (CLS) to estimate analyte concentration and apply a process of hypothesis testing to determine a goodness of fit metric[5]. The detected analyte peak shape is compared to a measured shape that is stored in a signature database. For the ricin detection analysis, one of the measurements was used to generate the signature database.

Generation of Signature Database Information

A representative dataset was chosen for generation of the database information for both standards and Ricin. This dataset was chosen somewhat arbitrarily, with the only condition being that it has reasonable peaks for both standards and analyte. Most of the other datasets could have been used since the shape of the ricin peak and the standards were consistent for most of the measurements. The sampling frequency for the data is10 Hz (this value has no effect on the analysis so long as all the data is collected at the same sampling frequency).

The following set of analysis parameters were used for peak detection (using ABS-PD): t_{min} = 50.0 seconds (500 samples), 2nd-degree polynomial smoothing with 21 samples (Savitzky-Golay filtering[6]), 5th degree polynomial for the background fit, 10 iterations, discrimination factor β = 3.0 and threshold ε = 5.0. Non-negative peak stabilization was turned on for this analysis.

Figure (1) shows the background corrected signal for the "red" channel for the standards which are identified as follows: peaks 2, 3, and 4 correspond to CCK, OVA, and BSA respectively. The standard peaks are represented by Gaussians in the signature database

The background-corrected analyte channel ("blue") is shown in figure (2) below. Peak 7 corresponds to Ricin which is represented by a cubic spline fit in the database file (note that two

overlapping Gaussians could also be used). This data also contains an SEB peak (peak 6), but this analyte will not be considered for this preliminary analysis.

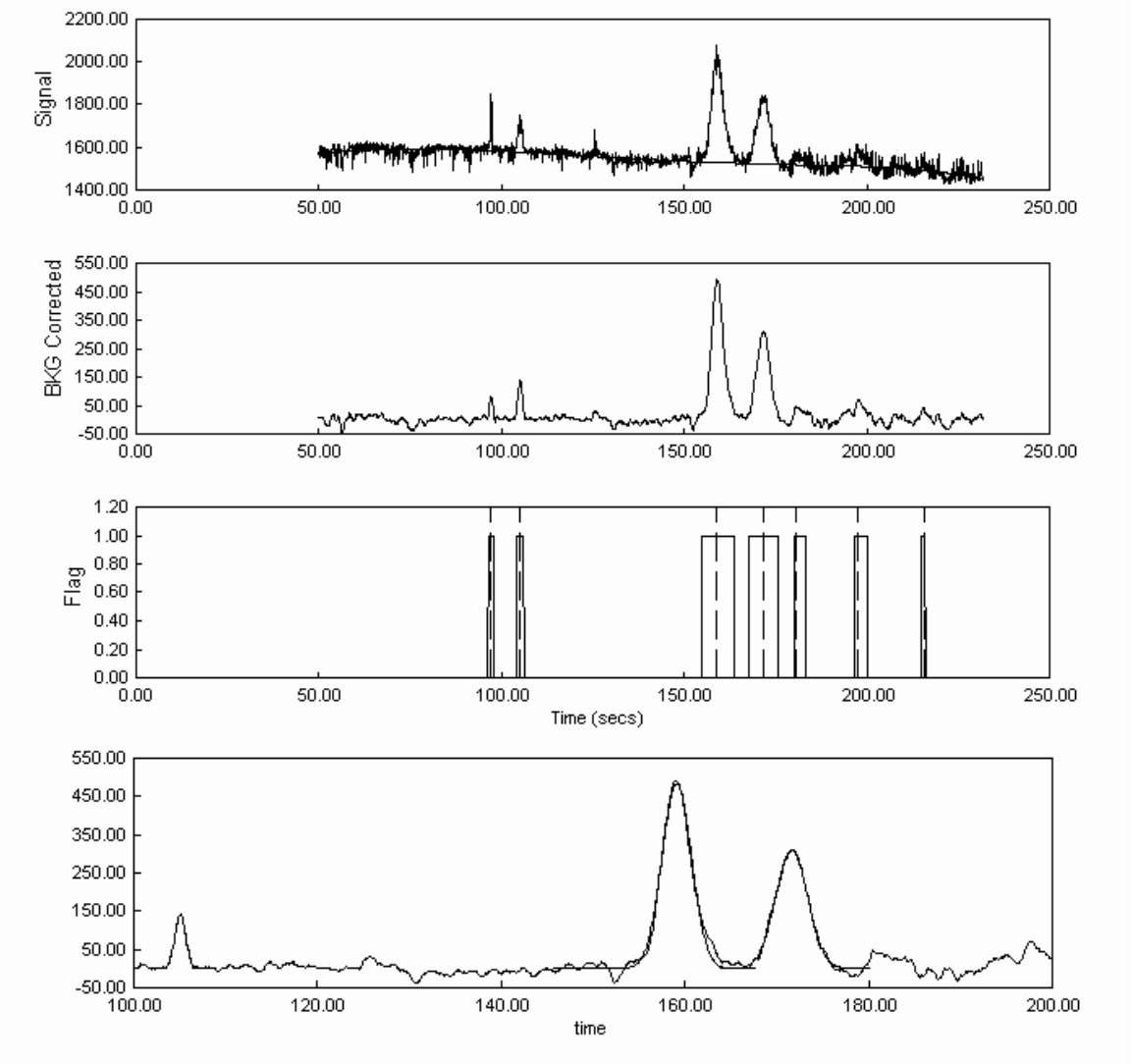

Figure (1). Peak detection and fitting for the standards ("red") channel for a representative measurement. This data was used for generation of the signature database. The top plot shows the original data along with the calculated background fit, the second plot shows the polynomial smoothed data after subtraction of the background and the third plots shows the detected peaks and their extent. The last plot shows Gaussian fits of the CCK, OVA, and BSA standard peaks respectively.

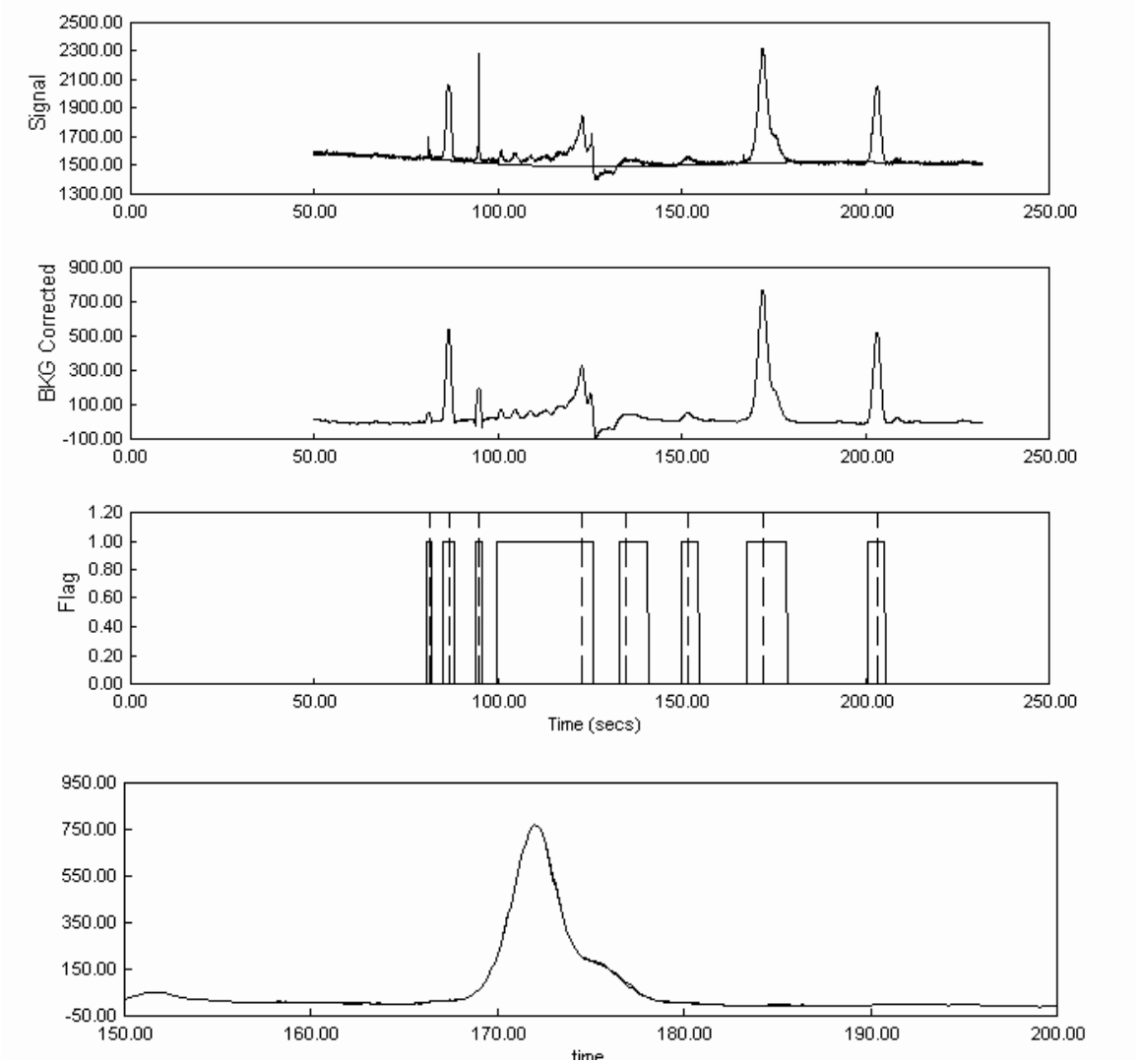

Figure (2). Peak detection and fitting for the analyte channel ("blue") for the same measurement used in Figure (1). The 7th detected peak corresponds to ricin. The bottom plot shows the cubic spline fit of the ricin peak along with the background-corrected and smoothed data.

Time Scale Correction

The three standards CCK, OVA, and BSA were used for a piece-wise linear time correction of analyte channel data. First the CCK peak was identified as the largest amplitude peak in a specified time window around the database time for CCK (a window of width of 30 seconds was used). The standards chromatogram is then shifted by an amount to line up the CCK peak with the database value. After this initial correction, the OVA and BSA peaks are identified and a piece-wise linear time correction function is calculated to match these standard times to the database values. The overall time shift correction is applied to the analyte channel.

For all 29 ricin measurements the three standard peaks were correctly identified. For 238 of 240 water sample measurements, all three standard peaks were also correctly identified. For one measurement the BSA peak was below the detection limit and for another measurement, the OVA and the BSA resulted in an overlapping peak which was not resolved by the overlapping peak algorithm. Some results of the time correction analysis will be shown in the next section

Removal of Noise Spikes

There are occasionally sharp spikes in the data due to air bubbles or other measurement related effects. With smoothing of the data these sharp peaks are broadened, and since they occur at random times in the data it is possible for such broadened peaks to cause false ricin detections. Such false detections are not likely to be called because of the peak shape matching that is done. However, it is more practical to remove such peaks before the data smoothing process.

The simple method chosen for removing such noise spikes is to run the ABS-PD algorithm before data smoothing and then peaks that are narrower than a specified width are removed from the data by setting the signal values in the peak region to be equal to the adjacent signal value. After this process, the corrected signal is smoothed and the ABS-PD algorithm is run once again to detect the actual peaks.

For this analysis, the noise peak removal process is only applied to the analyte channel, since we found that a few of the CCK peaks were also removed from the standards channel. This occurred for cases where the CCK peak amplitude was very small. For these cases the detected peak width was narrower than the true width because a significant part of the peak was below the detection limit set by the algorithm.

Another problem is that of noise spikes that occur within a true peak. This occurred in one dataset where a noise spike overlapped with the ricin peak. The smoothing in this case resulted in significant distortion of the ricin peak shape, resulting in decreased goodness of fit metric (signal-to-fit error ratio was smaller than the specified lower limit for the peak shape to be acceptable). For this analysis we will not attempt to filter noise spikes (due to bubbles or other phenomena) within valid peaks, however the affected data was excluded from the derived instrument response distribution. Additional filtering (for example using a derivative test; spikes will produce large derivative values and a threshold test is very effective at detecting them) can be used to correct for this deficiency.

III. Detection Analysis Results – Ricin Separations

There were 29 trials with Ricin at varying concentrations, with four replicates for each concentration (one concentration had five replicates). Figures (3-4) show two sample analyses results showing the background fitting and subtraction, detected peaks, time-corrected data and the calculated fit. The detected ricin amplitudes are shown in figure (5) for all the trials. At the lowest concentration of 7.4 nM (trials 22-25) no ricin peaks were detected. For the next lowest concentration of 14.8 nM (trials 26-29), ricin was detected for only one of the four measurements. The instrument response distribution normalized to the ricin concentration is shown in figure (6). Thus for trials 22-25 and 27-29 the resulting instrument response is below the detection limit for the set of parameters used in the detection algorithm (see figure (7) for the algorithmic detection limit based on noise and efficiency of background suppression). Also, the response for trial 17 is incorrect due to the noise spike that overlapped with the ricin peak. Thus trials 17, 22-25, and 27-29 will not be used in estimating the instrument response probability distribution.

For all 29 trials, the three standard peaks were identified correctly and their detected amplitudes are shown in figure (8). As seen in this figure the sensitivity of the standards channel is variable in a way that does not appear to be correlated with the analyte channel. Thus, for this analysis the signal amplitudes for the standards will not be used for correcting the calculated analyte concentrations. In general, for a 2-color system, using standards for analyte amplitude correction is not likely to be a useful option since the two channels use different lasers, optics and detectors. However, this is still a possibility if the instrument response of the two channels can be correlated with measured quantities in a reproducible manner.

The observed variability in the instrument response for the analyte channel, especially the large response observed in trials (17-20), indicates that the instrument is not optimized for most measurements. Understanding and addressing the sources of variability is expected to significantly improve the device performance and sensitivity. Additional performance improvement can also be achieved by optimization of the detection algorithm parameters.

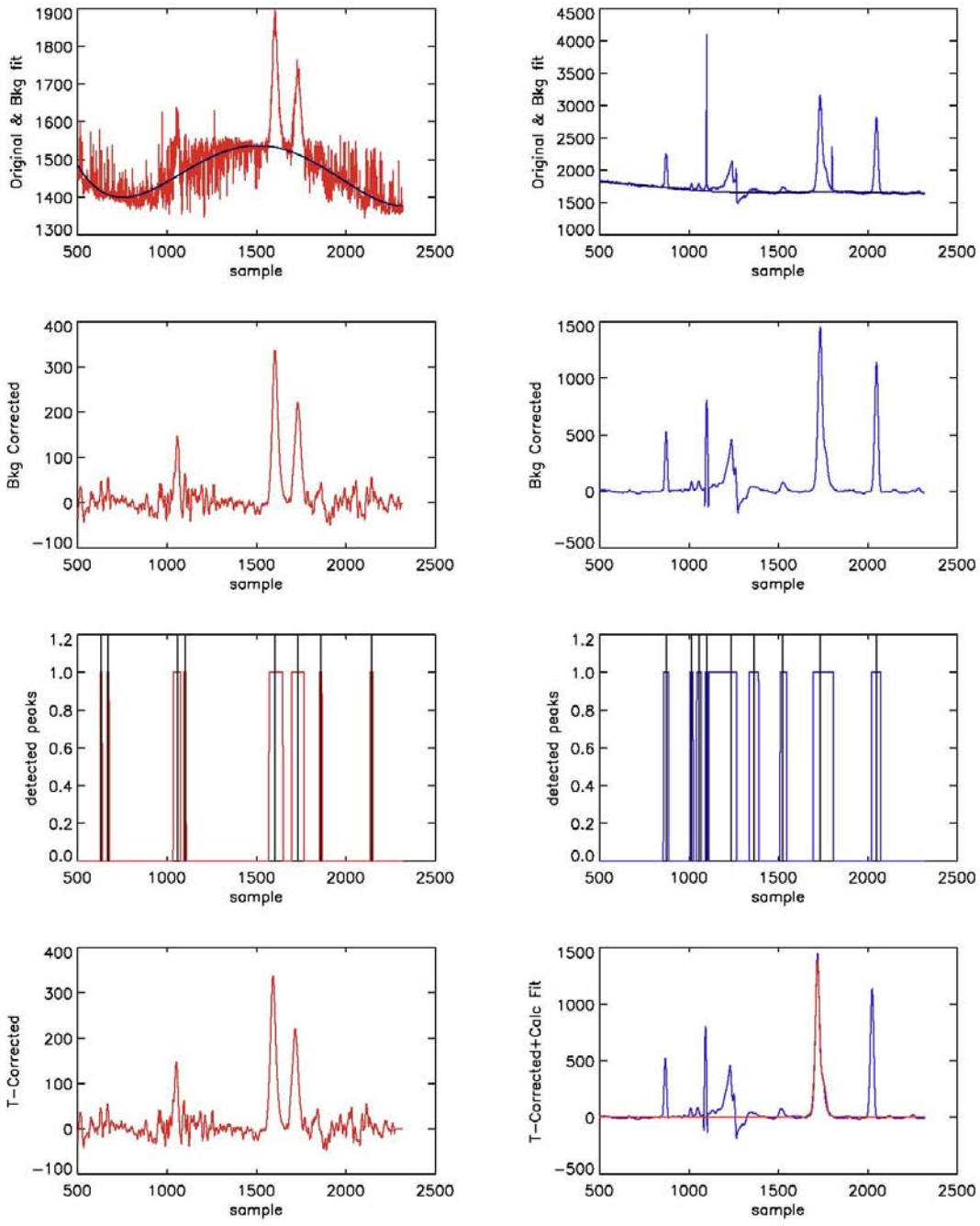

Figure (3). Results of analysis for data file "y06m02d15h14m17s56_stock3.txt" at a ricin concentration of 369 nM. The left plots are for the standards channel (red) and the right plots are for the analyte channel. From top to bottom the plots are: 1- Original data and background fit. 2- Smoothed data after subtraction of the background. 3- Detected peaks and their extent. 4- Time corrected data (blue) and the calculated analyte fit (red), which is ricin in this case. Note: the horizontal axis is shown in sample units (each sample corresponds to 0.1 seconds; total measurement time is about 230 seconds).

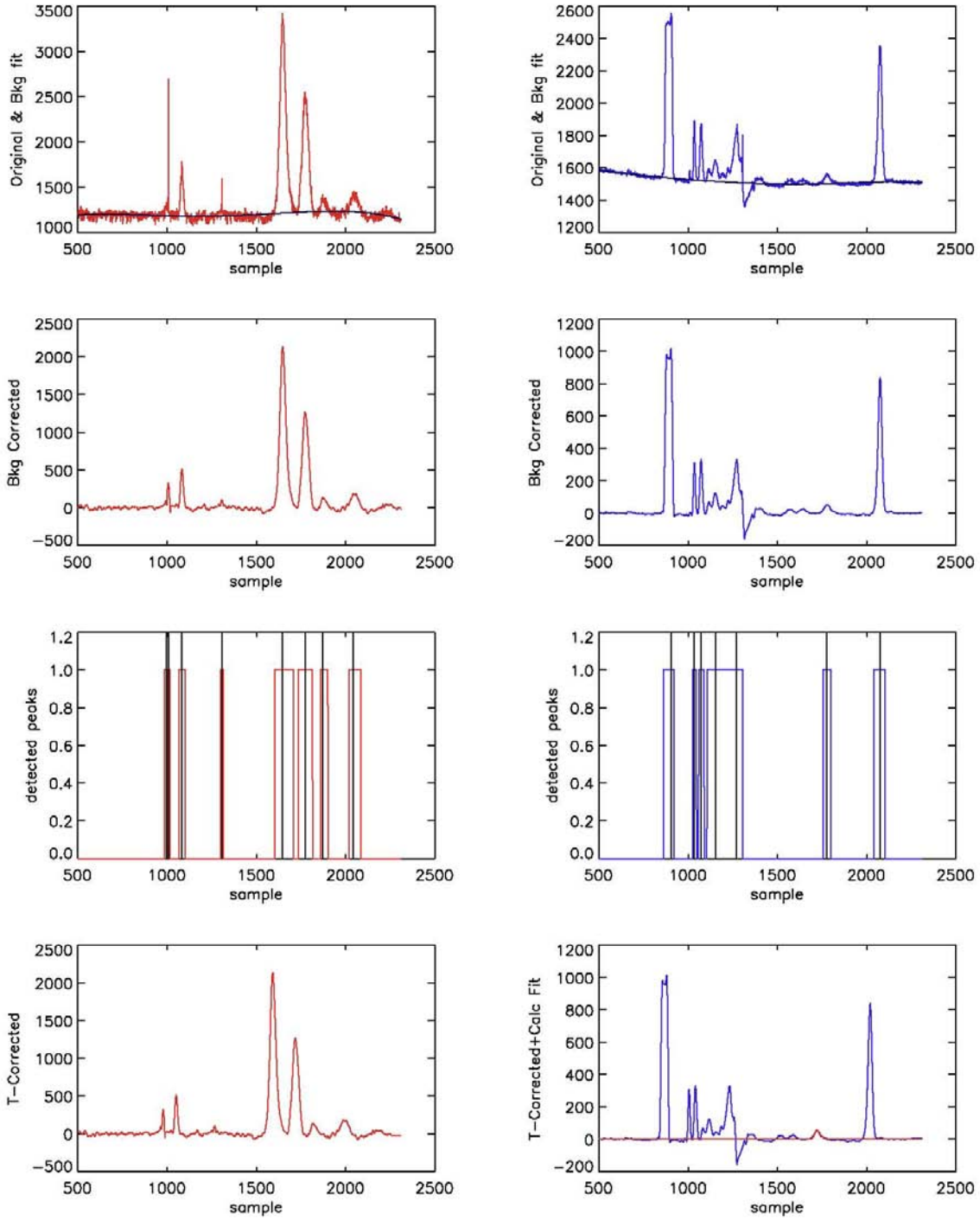

Figure (4). Results of analysis for data file "y06m02d16h18m31s07_stock9.txt" at a ricin concentration of 14.8 nM. The left plots are for the standards channel (red) and the right plots are for the analyte channel. From top to bottom the plots are: 1- Original data and background fit. 2- Smoothed data after subtraction of the background. 3- Detected peaks and their extent. 4- Time shift-corrected data (blue) and the analyte fit (red), which is ricin in this case. Note: the horizontal axis is shown in sample units (each sample corresponds to 0.1 seconds).

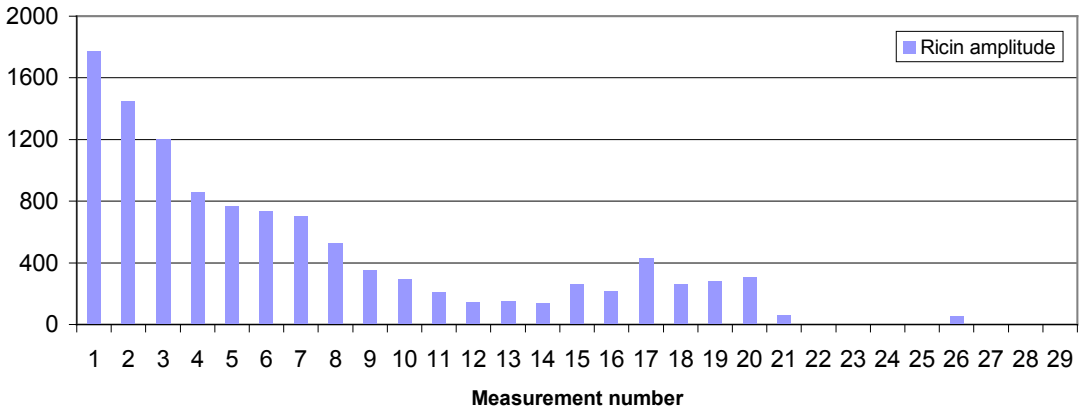

Figure (5). Detected ricin peak amplitudes for all the measurements. The concentrations for these trials are: 369 nM for measurements 1-4 (stock 3), 185 nM for 5-8 (stock 4), 92 nM for 9-12 (stock 5), 46 nM for 13-16 (stock 6), 23 nM for 17-21 (stock 7), 7.4 nM for 22-25 (stock 8), 14.8 nM for measurements 26-29 (stock 9).

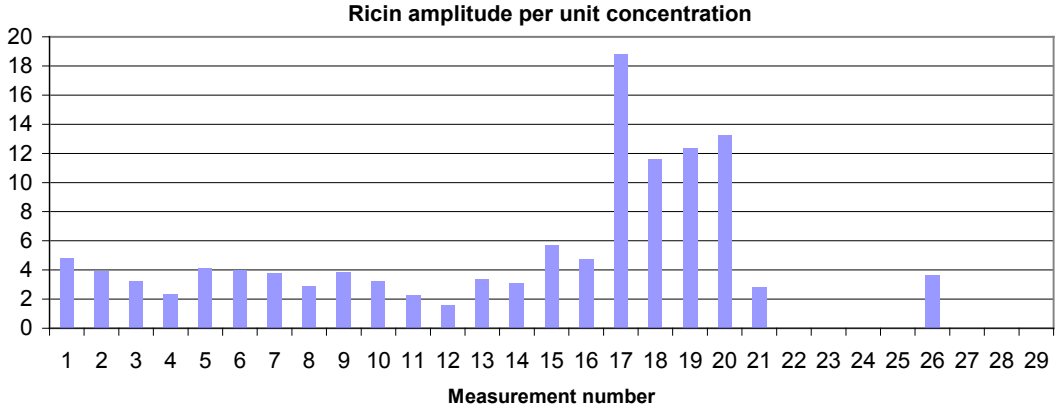

Figure (6). Instrument response for 29 ricin measurements. This is the detected ricin peak amplitude normalized to the concentration of the sample.

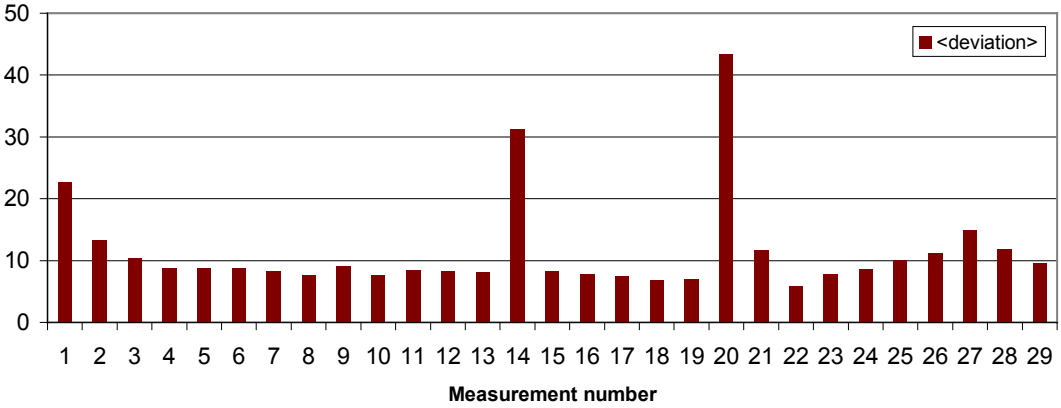

Figure (7). Average absolute deviation over background regions for all the ricin measurements. This quantity is used for setting the peak detection limit in the ABS-PD algorithm. Measurements 14 and 20 show abnormally large values due to high noise and background fit errors respectively.

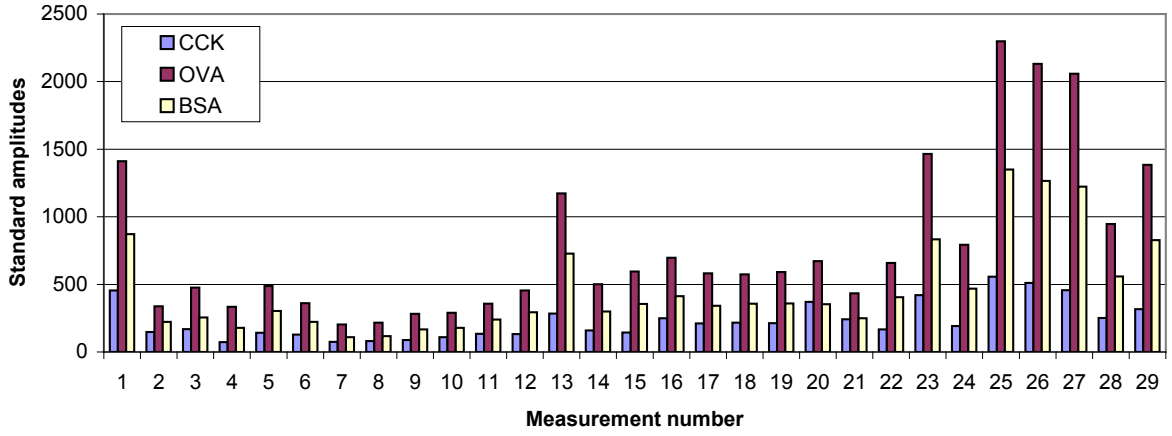

Figure (8). Detected s tandards amplitudes f or the ricin m easurements. The uni ts a re i n detector counts as directly obtained from the measurements.

IV. False Detections – Null Measurements

There were a large number of measurements of water samples without any ricin present. These measurements were obtained on a prototype device at one of the water utility stations over six consecutive da ys. A fter r emoval of t he r andom noi se s pikes t here w ere no de tections of a ny near-ricin peaks for the 240 measurements (using the same set of detection parameters as for the ricin measurements discussed earlier). For all but two of these measurements the three standards were correctly identified. F or one measurement the BSA peak was not detected and for another the B SA p eak w as n ot r esolved f rom t he O VA p eak. F or t hese t wo cas es, a l inear t ime correction be tween t he CCK a nd O VA pe aks i s us ed. N ote t hat b efore r emoval of t he noi se peaks, there were two cases where polynomial smoothing resulted in broadening of these peaks resulting in p eaks in th e r icin time r egion. The s hape id entification conditions us ed i n t he analysis would have ruled out these two cases as ricin detections. Also note that removal of the noise s pikes w as onl y applied t o t he a nalyte c hannel t o a void t he pos sibility of removing t he CCK pe ak f rom t he s tandards channel. F igures (9-10) s how s ample c hromatograms a nd analysis results for two representative measurements.

Figure (11) shows the detected standard amplitudes for all cases. Note that for measurement 156 the B SA pe ak w as not detected a nd for m easurement 240, i t w as not resolved f rom t he O VA peak. The overlapping peak detection algorithm should have been able to resolve the two peaks in t his cas e and w ill require s ome i nvestigation t o understand w hy t his w as not t he c ase. It is suspected that the parameters used did not allow sufficiently low contrast to distinguish the two peaks and therefore will require some adjustments.

Figure (11) shows significant variation of the response of the standards channel with time even though the concentrations of the standards were held constant for all the measurements. From this figure the degradation in response appears to be the same for all the standards. This could be caused by degradation in the fluorescence yield of the labeling dye, additional quenching, or can

be caused by changes in the alignment of some of the device optical components. These changes can be due to environmental effects such as temperature changes. As was pointed out earlier, these observations indicate that the device performance can be significantly improved and optimized by addressing the causes of variability. Additional performance improvement can be achieved by optimization of the detection algorithm parameters.

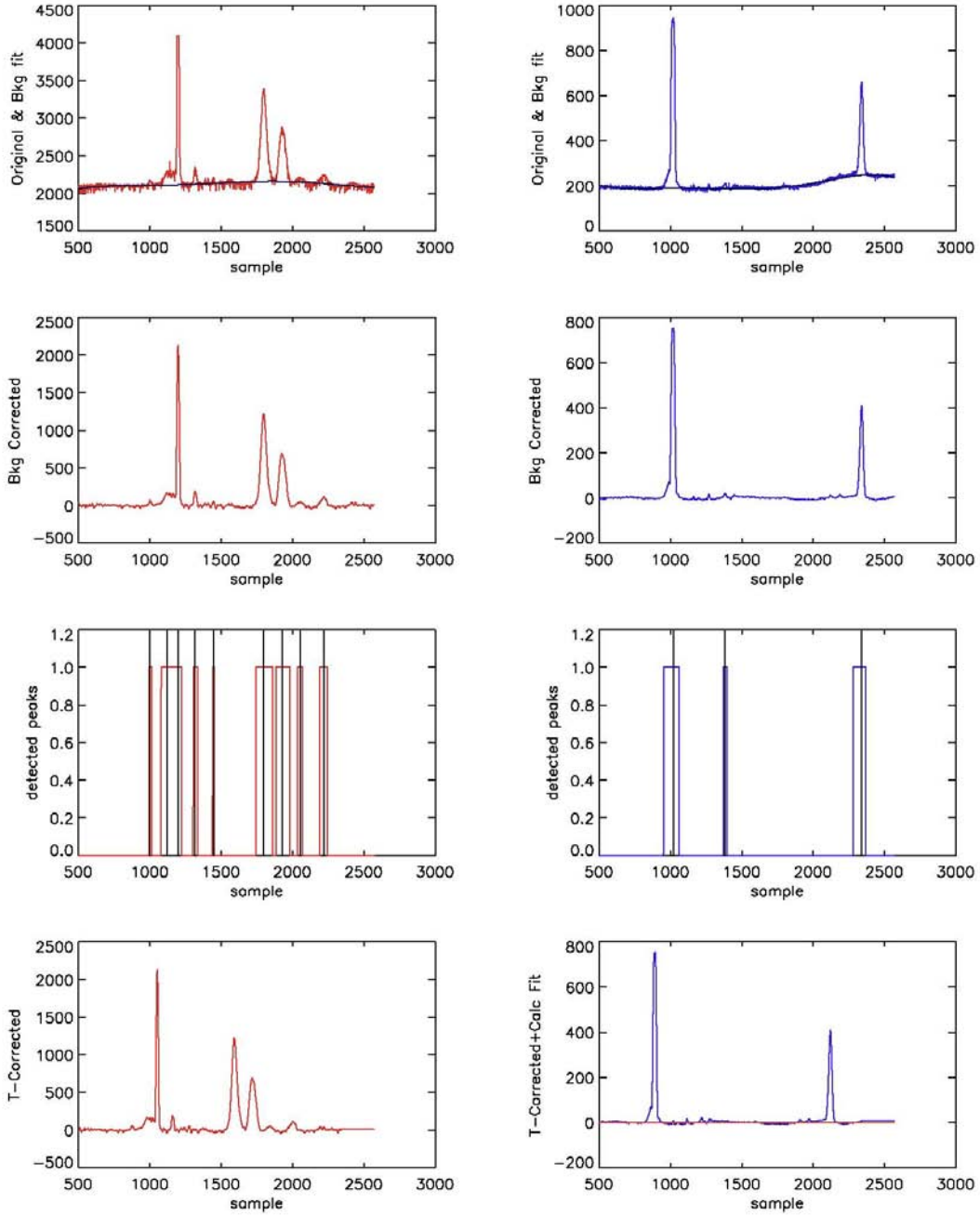

Figure (9). Automated detection analysis for CCWD data file " y06m02d16h11m23s23.txt". Note the time correction in the bottom plots is with respect to the standards in the signature database file. This is the first water sample measurement that was analyzed.

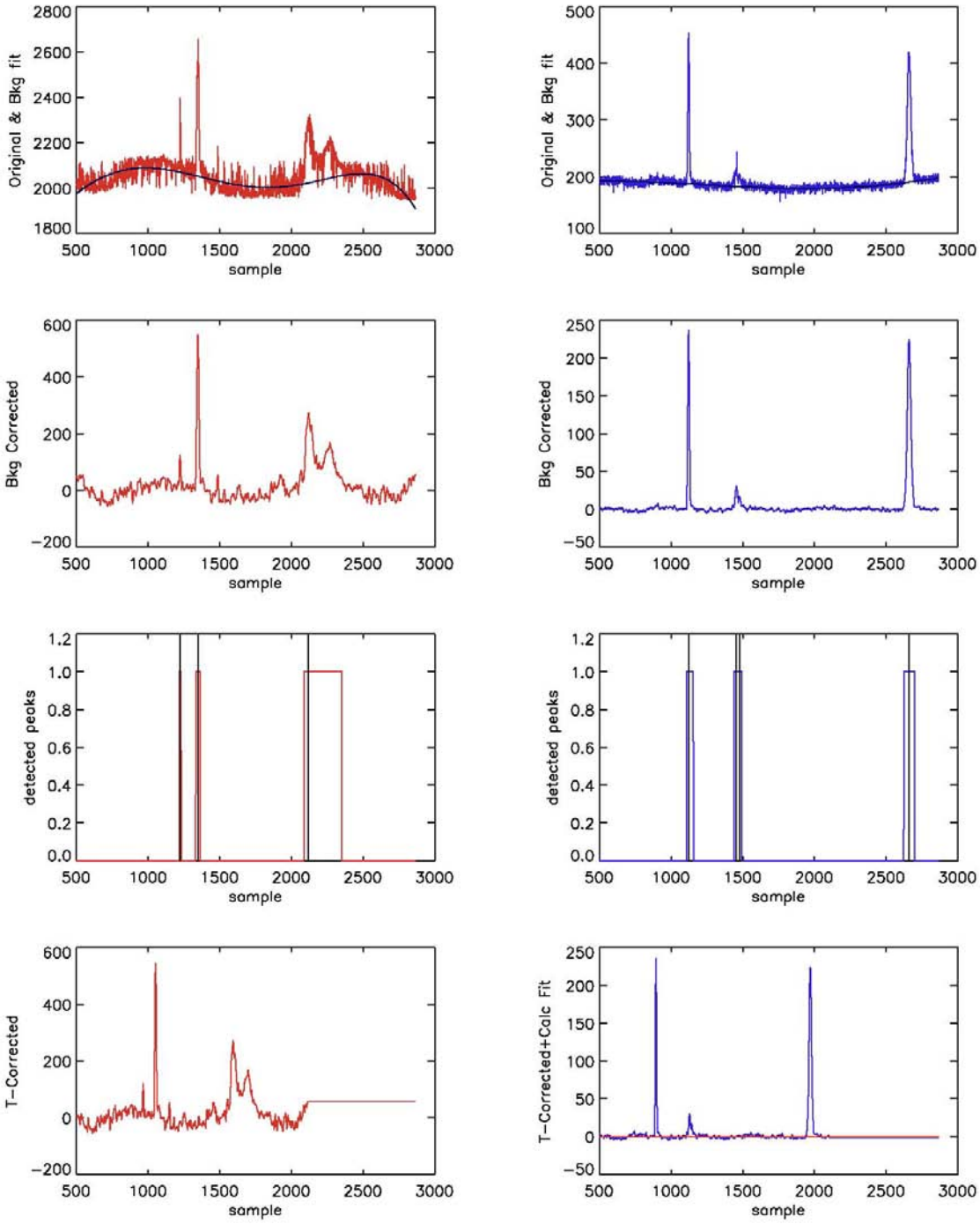

Figure (10). Automated detection analysis for CCWD data file "y06m02d21h11m02s53.txt" with problem of overlapping OVA and BSA peaks. This is the last CCWD water sample data that was analyzed. A change of algorithm parameters is expected to correct this deficiency.

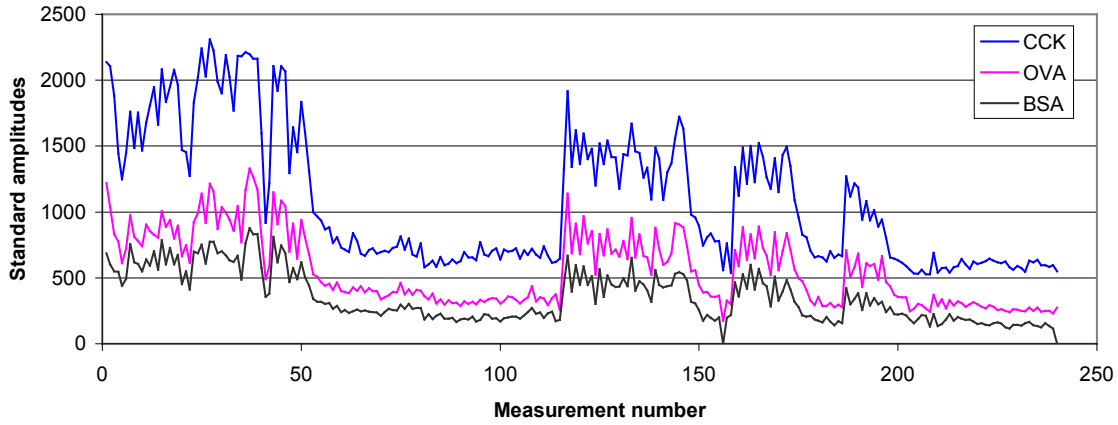

Figure (11). Amplitudes of standards for measurements of water samples. The dates for the measurements are: Feb 16: 1-26, Feb 17: 27-74, Feb 18: 75-122, Feb 19: 123-170, Feb 20: 171:218, Feb 21: 219-240. The units are in detector counts. The cases with zero amplitude for BSA denote measurements where the BSA standard was not detected for the parameters that were used.

V. Estimation of Detection Probability

The detection probability depends on the measurement device and also on the algorithm that is used to call detections. Although the amount of data available for the ricin-present measurements is not sufficient for a comprehensive analysis of detection probability, we will use the existing data along with the detection algorithm to obtain an estimate of this quantity.

The detection probability can be written as the product of two components: $P_D = (P_1\ P_2)\,P_3$, where P_1 is the probability that a peak is detected within a tolerance window for the analyte, P_2 is the conditional probability that once a peak is detected within the tolerance window, it is the analyte peak, and P_3 is the probability that the measured peak shape is the desired analyte peak shape, that is, it satisfies shape conditions set by the algorithm. Note that P_1 and P_2 are written out separately to handle the case with closely spaced analyte peaks. For this preliminary analysis we will assume that P_2 and P_3 are equal to unity. This is adequate for the present estimate since no interferents are expected to exist near the ricin peak and there is no sufficient information at this point to quantify the ricin peak shape variability. Thus the detection probability is estimated as the probability that the peak detection algorithm detects a peak within the defined tolerance window for ricin.

For each of the measurements, the ABS-PD algorithm is used to iteratively distinguish peak regions from background regions. Peak regions are defined as those regions where the measured signal (after polynomial smoothing) satisfies the following condition:

$$S(t) > \beta\ \ \delta + \varepsilon \qquad (1)$$

where $S(t)$ is the smoothed measured signal, δ is the averaged absolute deviation of the signal from the background fit in the iteratively determined background regions, β is the discrimination

factor (value of 3.0 i s us ed), a nd ε is a s tabilizing t hreshold va lue (ε = 5.0 was us ed f or t he current analysis). Note that δ is calculated for each measurement and thus the RHS of Eq. (1) is a user-defined detection limit. F or the ricin measurements, the calculated δ is shown in figure (7). T his qua ntity depends on t he m easurement noi se l evel a nd a lso on t he g oodness of background fit and thus in addition to dependence on measurements, it also depends on the ABS-PD parameters and how well this algorithm works. F or this estimate, only one set of ABS-PD parameters w ill b e co nsidered, n amely t he o ne u sed f or t he d etection an alysis (2^{nd}-degree centered polynomial smoothing with 21 samples, 5^{th}-degree polynomial fit of the background, 5 iterations, and with the non-negative peak constraint). F or detection probability estimates it is shown be low t hat onl y t he c umulative di stribution of δ is r equired a nd this w ill b e e stimated numerically based on results in figure (7). Note that this figure shows a couple of outliers which will be included in the distribution in order to avoid biasing the detection probability favorably.

Given an analyte measurement at a concentration C, the detection probability P_D is equal to the probability that the detected peak amplitude in the analyte tolerance window is larger than the calculated R HS o f E q. (1) f or t he cu rrent m easurement. Let t he q uantity $F($S;C) denote t he probability density that a μChemLab measurement with ricin present at a concentration C, will result i n a pe ak a mplitude e qual t o S , t hat i s, $F(S;C)\,\Delta S$ is th e p robability th at th e p eak amplitude i s be tween S a nd $S+\Delta S$ and es sentially d escribes t he i nstrument r esponse. The distribution F will be estimated directly from the measured data in figure (6). Given a ricin peak amplitude S and detection parameters β and ε , the probability of detection is given by:

$$P_D(S;\beta,\varepsilon) = \int_0^{(S-\varepsilon)/\beta} d\delta\ \varphi(\delta), \tag{2}$$

where t he uppe r l imit on t he i ntegral i s obt ained f rom E q. (1) a nd $\varphi(\delta)$ is t he pr obability density of a va lue δ for a m easurement. G iven a r icin co ncentration C, t he de tector r esponse probability distribution is used to obtain an overall probability of detection given by:

$$\begin{aligned} P_D(C;\beta,\varepsilon) &= \int_0^{\infty} dS\ F(S;C)\ P_D(S;\beta,\varepsilon) \\ &= \int_0^{\infty} dS\ F(S;C) \int_0^{(S-\varepsilon)/\beta} d\delta\ \varphi(\delta) \end{aligned} \tag{3}$$

Note that above we have assumed that the quantity δ is independent of the detection parameters β and ε. This is not always the case because background regions are affected by the choice of β and ε for c omplex ba selines. H owever, i t i s p ossible t o c alculate t he ba ckground f it us ing different values of β and ε than those used for calling a detection in order to insure convergence of the ABS-PD algorithm.

For c onstant m easurement c onditions, t he i nstrument r esponse i s a ssumed t o be l inear with analyte concentration. This can be inferred from figure (6) for the first 16 measurements. E ven though t here i s s ignificant va riability i n t he obs erved no rmalized r esponse, t here i s no clear

correlation of the normalized response with concentration. For measurements 17-20 the large change in instrument response is expected to be due to changes in the measurement conditions rather than an inherent nonlinear dependence of response on concentration. For better understanding of the instrument response a large number of controlled measurements at varying concentrations are required. For the present estimate a linear response will be assumed. Using this linear dependence the distribution $F(S;C)$ can be replaced with a new distribution:

$$\hat{F}(U) = C\ F(S;C) \qquad U = \frac{S}{C}$$

and Eq. (3) can be re-written as:

$$P_D(C;\beta,\varepsilon) = \int_0^\infty dU\ \hat{F}(U) \int_0^{(CU-\varepsilon)/\beta} d\delta\ \varphi(\delta)\,. \tag{4}$$

The desirable mode of operation for the sensor is clearly one that has the largest response per unit analyte concentration. This will result in a more favorable ROC curve, that is higher detection probability for a given false positive rate. However, until the operational conditions, method, and parameters that result in the large instrument response are established (could be as simple as better fluorescence yield for the dye), we opted to use all the available data to estimate the instrument response distribution for the current analysis. As noted previously trials 17, 22-25, and 27-20 will note be used.

Because of the small number of measurements, the process of estimating the instrument response distribution is not well defined and thus the procedure followed here is somewhat heuristic. First the cumulative distribution is calculated, that is the probability that the instrument amplitude (per unit concentration) is below a certain value. This is directly obtained from the data used in figure (6) and is shown below in figure (12). To accommodate the bimodal nature of the data two Gaussians were used with cumulative distribution given by:

$$\int_{-\infty}^{U} dU'\ \hat{F}(U') = \frac{1}{2}\left[1 + A_o\ erf\left(\frac{U-U_o}{\sqrt{2}\,W_o}\right) + A_1\ erf\left(\frac{U-U_1}{\sqrt{2}\,W_1}\right)\right] \tag{5}$$

A good fit was obtained using the parameters: $U_o = 3.1$, $W_o = 0.9$, $A_o = 0.85$, $U_1 = 11.9$, $W_1 = 1.0$, and $A_1 = 0.15$. It is important to note that this distribution is not a true statistical distribution because of the many systematic effects related to measurement variability. It is also expected that optimization of sensor parameters and operation (including steps such as sample preparation and injection) will result in a unimodal distribution at a higher amplitude than that for the smaller distribution in the figure below. For the performance assessment discussed later a ROC curve will be estimated separately for these two distributions.

For the ricin measurements the cumulative distribution of average deviation (see figure 7) is shown in figure (13) along with the analytical fit. The analytical fit is made up of the sum of two distributions given by:

$$\int_0^{\delta} d\delta' \, \varphi(\delta') = A\left[1 + erf\left(\frac{\delta - \delta_o}{\sqrt{2}\,\omega_o}\right)\right] + B\left[1 + \tanh\left(\frac{\delta - \delta_1}{\omega_1}\right)\right]\left(1 - e^{-\alpha\delta}\right) \qquad (6)$$

where the coefficients are estimated to be: $A = 0.38$, $\delta_o = 7.6$, $\omega_o = 1.3$, $B = 0.12$, $\delta_1 = 8.0$, $\omega_1 = 4.0$, and $\alpha = 0.06$. The first part of Eq. (6) is the contribution from a Gaussian and the second part represents a tail. Again, because of variability of baselines and the complex nature of how the average deviation depends on the data and the ABS-PD algorithm, it is not expected that the distribution represented by Eq. (6) will hold when large numbers of datasets are collected. In fact a significantly different distribution of the average deviation is obtained for the CCWD water sample measurements - see figure (14) below and the discussion in the following section. For this analysis we will use Eq. (6) with the understanding that significant improvement (lowering of the average deviation) is expected for optimized sensor operation. This would lead to lower detection limits and thus improved detection probability.

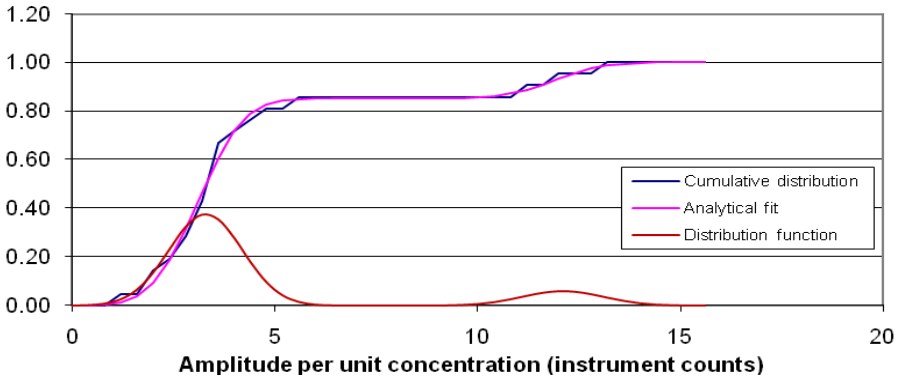

Figure (12). Cumulative distribution of the instrument response as a function of the signal amplitude per unit concentration for ricin. This plot also shows the analytical fit using two integrated Gaussians and the resulting distribution. The Gaussian parameters are: $U_o = 3.1$, $W_o = 0.9$, and $A_o = 0.85$ for the first and $U_1 = 11.9$, $W_1 = 1.0$, and $A_1 = 0.15$ for the second.

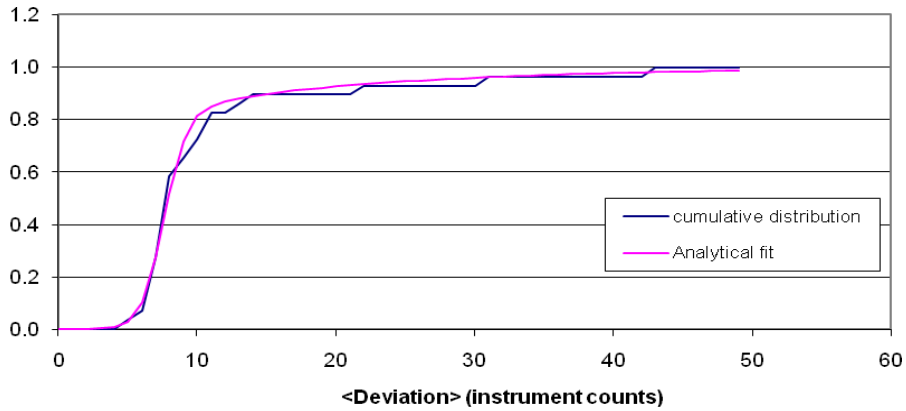

Figure (13). Measured and analytical representation of the cumulative distribution of the average deviation (δ) for the ricin measurements.

VI. Estimation of False Positive Probability

Analyte detection is possible only when a peak is detected within a specified tolerance window for the analyte. In addition, the peak shape has to satisfy certain goodness of fit criteria with respect to the analyte peak shape in the signature database. Therefore, in the absence of background interferents, the probability of false positives is expected to be very low. This is indeed the case for the 240 measurements of the CCWD water samples for which no ricin detection was made. For this initial estimate there is no background interferent data available and therefore such interferents will not be considered as contributors to false positives.

In the absence of background interferents, false positives are possible only due to baseline peaks (instrument-related) or baseline suppression errors that result in such peaks. Again as noted previously, it is unlikely that such peaks will have a shape similar to the signature shape for the analyte in question. At this point the shape criteria for ricin have not been completely defined due to the limited amount of data available (only one shape defined in the database) and also due to the fact that different species of ricin might have different shapes. Therefore, for estimating the false positive probability we use a very simple and crude method that does not utilize the peak shape as outlined below. This method should provide a useful estimate with the expectation that ricin will have several varieties with different peak shapes.

The null data (CCWD measurements) is used to calculate the area resulting from baseline suppression errors in the ricin time domain and then an effective amplitude for a hypothesized peak is calculated based on the signature database area and amplitude for ricin as:

$$A_{effecitve} = \left(\frac{A_{ricin}}{Area_{ricin}} \right)_{Database} \sum_{j} \left[S(j) - f_{bkg}(j) \right] \tag{7}$$

where the sum over (j) is over the ricin peak extent, S is the measured signal after polynomial smoothing, and f_{bkg} is the calculated fit of the background. The distribution of $A_{effective}$ is then estimated using the 240 CCWD measurements. Further assuming that such baseline errors will have a shape similar to that of ricin (including shapes for all possible varieties), we can estimate the false positive probability as a function β and ε, as was done for the detection probability above. For more detailed analysis the probability that baseline errors would result in a peak shape similar to that of ricin will need to be estimated. The conditions on what is an acceptable shape for calling a detection will also need to be determined based on shape variability due to measurement variance as well as variants of ricin. It should be noted that by not using the shape information fully, the false positive rate due to background suppression errors will be overestimated in this analysis.

Figure (14) shows the calculated $A_{effective}$ as given by Eq. (7) and the average deviation for the 240 water sample measurements. The cumulative distributions of the average deviation and effective amplitude are shown in figures (15-16) along with analytical fits. Note that the effective amplitude is calculated after the time correction of measured data.

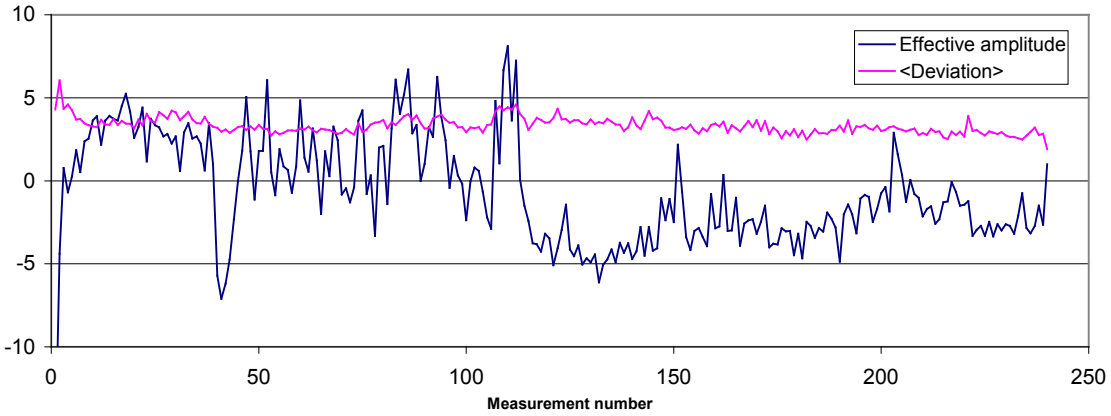

Figure (14). Effective ricin amplitude in instrument counts (based on background suppression errors) and the calculated average deviation for the CCWD water sample measurements. A total of 240 measurements were used.

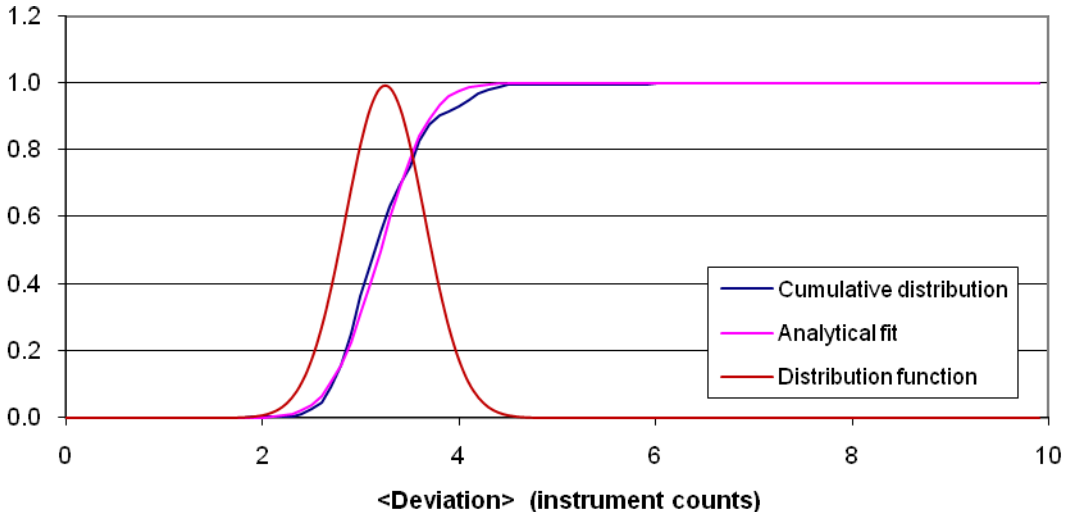

Figure (15). Cumulative probability distribution of the average deviation between polynomial smoothed signal and calculated background fit in background regions. This plot also shows the analytical fit to an integrated Gaussian and the resulting Gaussian distribution. The Gaussian parameters are S_o = 3.2 and W = 0.4.

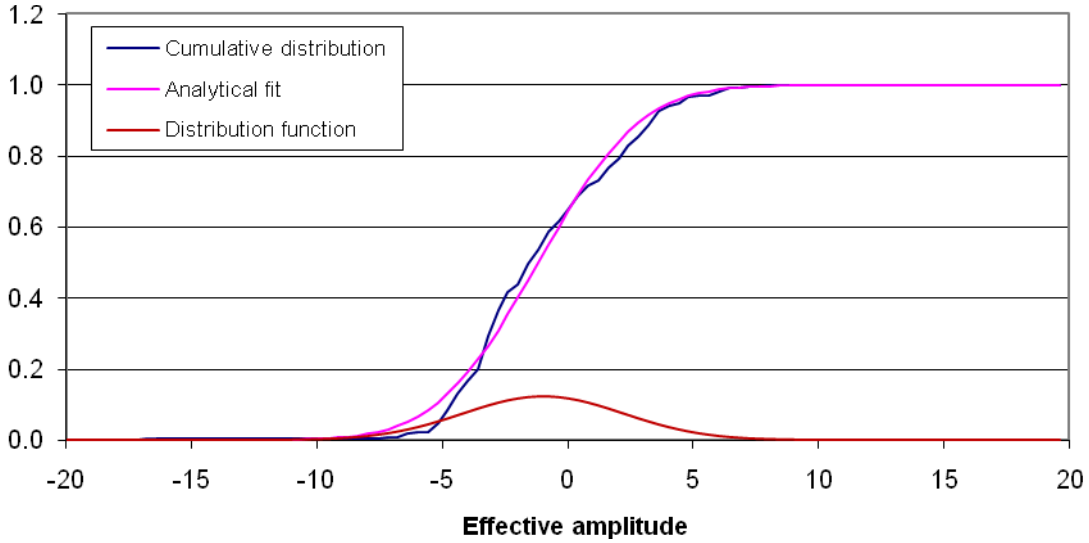

Figure (16). Cumulative probability distribution for the effective signal amplitude in the ricin time domain. This plot also shows the analytical fit to an integrated Gaussian and the resulting Gaussian distribution. The Gaussian parameters are $A_o = -1.2$ and $W = 3.2$. Note that as the number of measurements becomes large, we expect that A_o will have a limit equal to zero.

For a given measurement without the analyte present, the probability of a false detection is estimated as the probability that the effective amplitude in the time domain of the analyte of interest is larger than overall detection limit given by Eq. (1). Thus as was obtained for the detection probability in Eq. (3), the overall probability of a false detection denoted by P_{FD} is given by:

$$P_{FD} = \int_0^\infty dA\, \Psi(A) \int_0^{(A-\varepsilon)/\beta} d\delta\, \varphi(\delta) \qquad (8)$$

where $\Psi(A)$ is the distribution of calculated effective amplitudes shown in figure (16) and $\varphi(\delta)$ is the distribution of average deviation discussed previously and shown in figure (15). Given values of the detection algorithm parameters β and ε, and the device performance characteristics set by the distributions $\Psi(A)$ and $\varphi(\delta)$, the false detection probability can be estimated by using Eq. (8). Again we note that this estimate does not take into account the peak shape which can be used to rule out false detections. It also does not account for the effect of background interferents. Until the shape criteria for the different forms of ricin as well as measurement variability are determined, and possible interferents identified, the assumptions made here are not unreasonable.

VII. Performance Assessment - Receiver Operating Characteristics

The preliminary assessment of the UWS instrument for ricin detection will be represented in the form of Receiver Operating Characteristic (ROC) curves. The form of the curves that will be used is the detection probability (P_D) vs. the probability of false detections (P_{FD}). Although the horizontal axis is the P_{FD}, it actually represents instrument performance characteristics and detection algorithm parameters that result in the specific P_{FD}. This should clarify the use of the axes for these curves given that P_D measures detection probability when the analyte is present while P_{FD} is for cases when the analyte is not present.

Figures (17-18) show two sets of ROC curves at a few ricin concentrations. For these curves the value of the threshold parameter ε is fixed at 5.0 (value used for the detection analysis and has units of detector counts) and the discrimination factor β is varied between 1 and 10. Equations (4) and (8) along with the estimated cumulative distributions are used to calculate P_{FD} and P_D. The two figures are for the two Gaussian distributions of detector response represented by the bimodal distribution in Eq. (5).

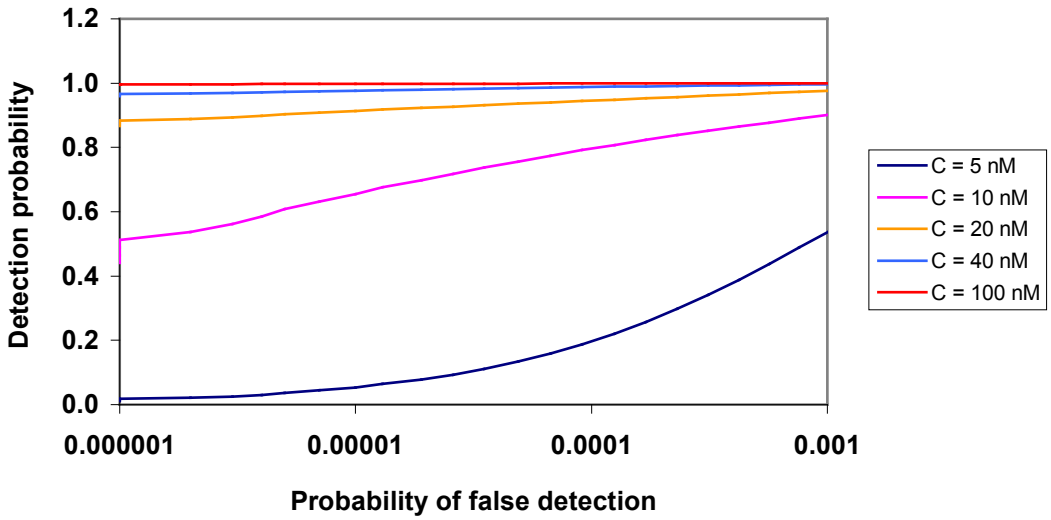

Figure (17). ROC curve for μChemLab detection of ricin using the smaller detector response corresponding to measurements 1-16, 21 and 26.

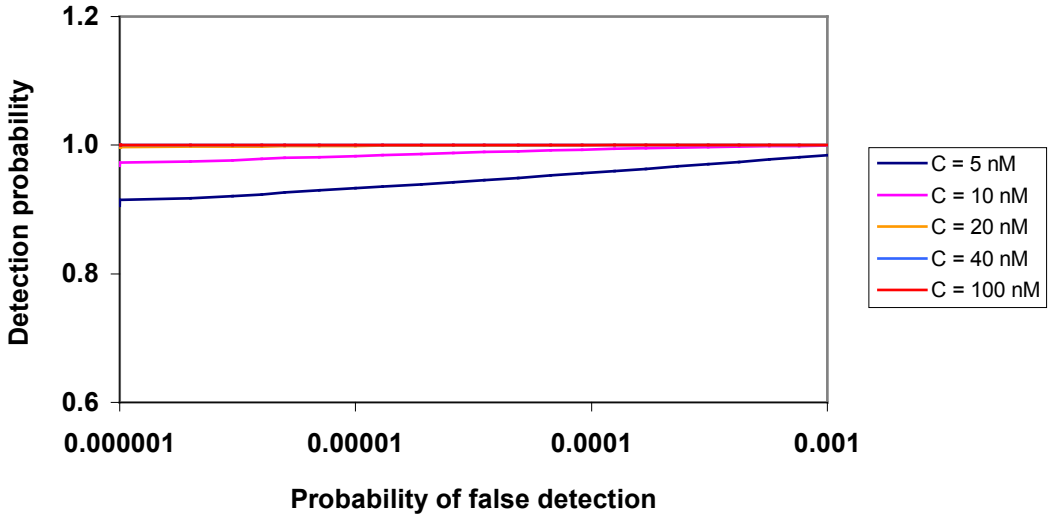

Figure (18). ROC curve for μChemLab detection of ricin using the larger detector response corresponding to measurements 18-20.

VIII. Summary and Conclusions

This report presented some performance assessment estimates for the UWS device based on a limited number of measurements. Assessment of the detection probability was based on laboratory measurements of ricin at varying concentrations. The probability of false detection was estimated based on null measurements at the CCWD water utility. A probability of detection of 0.9 for ricin at 5 nM was estimated for a false positive probability of $1x10^{-6}$.

We conclude that the UWS employing μChemLab technology is effective at detecting ricin in municipal water supplies. These conclusions should be considered preliminary because of the limited number of tests that were conducted. Also, because the measurements showed significant variability in the instrument response (for both analyte and standards channels) we conclude that the device was not operating at optimum conditions. Therefore, significant improvements in sensitivity can be expected for an optimized device. Further analyses including possible interferents are needed for better estimation of the false positive probability.

Additional improvements in performance are possible with optimization of the detection algorithm parameters. This can be investigated in the future. The analysis methods developed for this assessment can also be extended to other devices utilizing similar technology.

References

(1) Fruetel, Julia A., Ronald F. Renzi, Victoria A. VanderNoot, James Stamps, Brent A. Horn, Jay A.A. West, Scott Ferko, Robert Crocker, Christopher G. Bailey, Don Arnold, Boyd Wiedenman, Wen-Yee Choi, Daniel Yee, Isaac Shokair, Ernest Hasselbrink, Philip Paul, David Rakestraw, and Debbie Padgen, (2005) *Electrophoresis*, **26,** 1144 – 1154.

(2) Renzi, Ronald F. James Stamps, Brent A. Horn, Scott Ferko, Victoria A. VanderNoot, Jay A.A. West, Robert Crocker, Boyd Wiedenman, Daniel Yee and Julia A. Fruetel, Hand-Held Microanalytical Instrument for Rapid Chip-Based Electrophoretic Separations of Proteins, (2004) *Analytical Chemistry*, **77**, (2005), 435-441.

(3) Julia A. Fruetel, Jason A.A. West, Bert J. Debusschere, Kyle Hukari, Todd W. Lane, Habib N. Najm, Jose Ortega, Ronald F. Renzi, Isaac Shokair, Victoria A. VanderNoot, Rapid Identification of Viruses using Microfluidic Protein Profiling and Bayesian Classification, *Analytical Chemistry*, (2008), **80**, 9005-9012.

(4) Isaac. R. Shokair, "Adaptive Background Suppression and Peak Detection Algorithm for Chemical Analysis Applications", Sandia National Laboratory Report SAND2002-8143, March 2002.

(5) I. R. Shokair, C. Springer, D. C. Roe, J. A. Fruetel, V. A. VanderNoot, and T. M. Berg, "Analysis Modeling and Data Fusion for Chemical/Biological Sensor Arrays", Sandia National Laboratory Report SAND-2002-8144, March 2002.

(6) A. Savitzky and M.J.E. Golay, "Smoothing and Differentiation of Data by Simplified Least Squares Procedures", Analytical Chemistry **36** (8), pg 1627-1639, 1964. See also W. H. Press, B. P. Flannery, S. A. Teukolsky, and W. T. Vetterling, Numerical Recipes, Cambridge University Press, 1986. Also, Numerical Recipes in C, 1992.

Distribution:

1	MS 9004	J. M. Hruby, 8100	(electronic copy)
1	MS 9004	S. P. Gordon, 8101	(electronic copy)
1	MS 9004	D. L. Lindner, 8120	(electronic copy)
1	MS 9104	W. R. Bolton, 8123	(electronic copy)
1	MS 9104	I. R. Shokair, 8123	(electronic copy)
1	MS 9104	L. R. Thorne, 8123	(electronic copy)
1	MS 9291	B. L. Haroldsen, 8123	(electronic copy)
1	MS 9291	N. J. Gleason, 8125	(electronic copy)
1	MS 9291	A. K. Singh, 8621	(electronic copy)
1	MS 9292	R. W. Crocker, 8125	(electronic copy)
1	MS 9292	G. W. Foltz, 8125	(electronic copy)
1	MS 9292	J. A. Fruetel, 8125	(electronic copy)
1	MS 9292	R. F. Renzi, 8125	(electronic copy)
1	MS 9292	V. A. VanderNoot, 8621	(electronic copy)
1	MS 0899	Technical Library, 9536	(electronic copy)